JOURNAL OF SOLID STATE CHEMISTRY **130,** 81–89 (1997)
ARTICLE NO. SC977271

Surface Segregation and Oxygen Vacancy Ordering in Defect Pyrochlores

Ismunandar and Brendan J. Kennedy

School of Chemistry, The University of Sydney, New South Wales 2006, Australia

and

Brett A. Hunter

Australian Nuclear Science and Technology Organisation, Private Mail Bag 1, Menai, New South Wales 2234, Australia

Received October 1, 1996; in revised form December 24, 1996; accepted January 7, 1997

The bulk structure and surface composition of the two oxygen defect pyrochlore oxides $Pb_2(M_{1.5}W_{0.5})O_{6.5}$ (M = Ti, Sn) have been studied in order to determine the relationship between anion vacancies, electrical conductivity, cationic mobility, and surface segregation in pyrochlore oxides. The bulk structures were refined by Rietveld analysis combining powder neutron and X-ray synchrotron diffraction data. The two oxides are isostructural, space group $F\bar{4}3m$ (No. 216), with $a = 10.3501(1)$ Å for M = Ti and $a = 10.6051(2)$ Å for M = Sn, where the M and W atoms are randomly distributed in the 16*e* site and oxygen-vacancy ordering occurs on the pyrochlore type 8*b* sites. In both cases the Pb cation is surrounded by seven oxygen atoms in a compressed scalenohedral arrangement where the eighth vertex is occupied by the Pb 6*s* lone pair electrons. In $Pb_2(Ti_{1.5}W_{0.5})O_{6.5}$, the Pb atoms are displaced by 0.032(8) Å along the [111] direction toward the associated vacancy, while in the larger $Pb_2(Sn_{1.5}W_{0.5})O_{6.5}$ the Pb cation is not displaced away from the ideal 16*d* site position. This difference is a consequence of the Pb–O bonding requirements. The surface composition of both oxides is identical to that of the bulk composition. By comparison with other studies these results demonstrate that electrical conductivity is a critical factor in determining surface enrichment by the potentially mobile A-type cations in pyrochlore oxides. © 1997 Academic Press

INTRODUCTION

There is considerable current interest in the structure and properties of defect pyrochlores, driven in part by their potential technological importance in a diverse range of applications including fast ion conductors, electrocatalysts, resistors, sensors, etc. (1). The interest has been further stimulated by the discovery of giant magnetoresistance (GMR) in $Tl_2Mn_2O_{7-y}$ (2). The wide spread occurrence of oxygen defects in pyrochlore-type oxides can be understood if the cubic $A_2B_2O_6O'$ pyrochlore structure is viewed as two interpenetrating networks, the first a corner-shared B_2O_6 octahedra network and the second an A_2O' network similar to the anticristobalite Cu_2O network. The B_2O_6 network is fairly rigid and does not interact strongly with the A_2O' network and as a result cation and/or anion vacancies in the A_2O' network do not significantly reduce the stability of the lattice. A second form of nonstoichiometry often observed in pyrochlore type oxides is the partial substitution of the A-type cation onto the B site. This appears to be most prevalent when the A-type cation is a post transition metal such as Pb and Bi (3).

In the $A_2B_2O_6O'$ pyrochlore structure, space group $Fd\bar{3}m$, all the atoms are in special positions. There is only one positional parameter, x, which describes the position of the oxygen atoms on the 48*f* site (x, 0.125, 0.125). The geometry of both the A and B cations is dependent on the value of the single variable oxygen positional parameter. The relatively low X-ray scattering power of oxygen means that neutron diffraction is the preferred method for the accurate determination of this parameter. The structure of a number of oxygen defect pyrochlore oxides of the type $A_2B_2O_{7-y}$, where A is a post-transition metal and $y = 0.5$, including $Pb_2Ru_2O_{6.5}$ (4), $Pb_2(TiSb)O_{6.5}$ (5), and $Pb_2Ir_2O_{6.5}$ (6) have now been the subject of powder neutron diffraction studies and in all cases have shown evidence for oxygen vacancy ordering accompanied by a displacement of the A-site cation (4–6). The structures of these oxides are best described in the cubic space group $F\bar{4}3m$, that allows for both oxygen vacancy ordering and displacement cations away from the special positions. If y is less than 0.5 then the oxides invariably adopt a regular pyrochlore structure and, as seen for $Bi_2Ru_2O_{6.9}$ and $Bi_2Ir_2O_{6.9}$ (6, 7), the oxygen vacancies are only on the O′ site.

0022-4596/97 $25.00
Copyright © 1997 by Academic Press
All rights of reproduction in any form reserved.

Studies of the electrocatalytic properties of the metallic oxides $Pb_2Ru_2O_{6.5}$ and $Bi_2Ru_2O_{6.9}$ have shown (8, 9) that surface segregation of the *A*-type cation was much greater in $Pb_2Ru_2O_{6.5}$ than in $Bi_2Ru_2O_{6.9}$, and it was suggested that the stability of these oxides is related to the number and arrangement of the oxygen vacancies seen in powder neutron diffraction studies of these two oxides (4, 7). Likewise the surface of the metallic oxide $Pb_2Ir_2O_{6.5}$ (6) was noticeably Pb rich. More recently, investigations of the structural and surface properties of some $Bi_3M_3O_{11}$-type oxides demonstrated Bi surface enrichment to occur in the metallic oxide $Bi_3Ru_3O_{11}$ but not in the electrically insulating oxides $Bi_3(MSb_2)O_{11}$ (M = Al, Ga) (7, 10) suggesting that there may be a relationship between the metallic conductivity of the metal oxide and the ionic mobility of the *A*-type cation. This leaves two possible causes of the enhanced surface enrichment by Pb in $Pb_2M_2O_{6.5}$ (M = Ru, Ir) — oxygen vacancy ordering or metallic conductivity. The aim of the present work is to establish if these effects can be further quantified by a study of a nonmetallic oxide where oxygen vacancy ordering occurs.

The two nonmetallic oxides $Pb_2(Sn_{1.5}W_{0.5})O_{6.5}$ and $Pb_2(Ti_{1.5}W_{0.5})O_{6.5}$ were first described in 1964 (11) as having a cubic pyrochlore structure. In 1993 Wakiya suggested that the correct space group for these oxides is $F\bar{4}3m$, although, as he also pointed out, even if half the O′ sites are vacant, anion-vacancy ordering does not always occur (12). As part of a wider study of the interrelationship between chemical reactivity, surface composition, and defect ordering in pyrochlore oxides it was decided to investigate the bulk structure and surface compositions of $Pb_2(Sn_{1.5}W_{0.5})O_{6.5}$ and $Pb_2(Ti_{1.5}W_{0.5})O_{6.5}$. These nonmetallic oxides provide a means to compare the structural and surface chemistry of the metallic and nonmetallic pyrochlores containing a large number of anion vacancies. Bulk structures were determined using combined neutron and synchrotron X-ray powder diffraction (ND and XRD) methods. To accurately and precisely describe both forms of nonstoichiometry, i.e., anion defects and possible disorder of the cations, using powder diffraction methods it is necessary to use a combination of X-ray and neutron diffraction to ensure suitable contrast in scattering powers of all the elements. The surface composition was characterized using scanning electron microscopy (SEM) and X-ray photoelectron spectroscopy (XPS). The results of these studies are reported in this paper.

EXPERIMENTAL

Polycrystalline samples of $Pb_2(Ti_{1.5}W_{0.5})O_{6.5}$ and $Pb_2(Sn_{1.5}W_{0.5})O_{6.5}$ were prepared by the solid state reaction of stoichiometric quantities of PbO (Aldrich, 99.99%), WO_3 (Aldrich, 99.995%), and TiO_2 (Aldrich, 99.999%) or SnO_2 (Aldrich, 99.99%). The intimately mixed materials were heated in air at 700°C for 12 h, 750°C for 24 h, and finally at 800°C for 24 h for $Pb_2(Ti_{1.5}W_{0.5})O_{6.5}$ and at 900°C for 24 h and then at 1000°C for 24 h for $Pb_2(Sn_{1.5}W_{0.5})O_{6.5}$, with regrinding after each heating step. The formation of single phase pyrochlore type oxides was confirmed by powder XRD measurements at room temperature on a Siemens D5000 diffractometer. Scanning electron microscopy and energy dispersive X-ray analysis (EDA) were performed on a Phillips SEM 505 equipped with an EDAX PV9900 energy dispersive analyzer. For the microscopy studies the samples were coated with either Pt or C to minimize charging effects.

The powder neutron diffraction patterns were recorded in 0.05° steps in the range $0° < 2\theta < 156°$ at room temperature using neutrons of wavelength 1.4928 Å on the high-resolution powder diffractometer (HRPD) (13) at the HIFAR reactor operated by the Australian Nuclear Science and Technology Organisation (ANSTO). The lightly ground sample was contained in a thin-walled 16-mm-diameter vanadium can that was slowly rotated during the measurements to minimize the effects of preferred orientation. The synchrotron diffraction patterns were recorded in 0.01° steps at room temperature using X rays of wavelength 0.99756 Å in the range $10° < 2\theta < 125°$ on the Australian National Beamline Facility (ANBF) powder diffractometer on BL-20B at the KEK Photon Factory, Japan, using image plates (IP) as detectors. In each case the lightly ground sample was housed in a 0.5-mm-diameter glass capillary that was rotated during the measurements. A full description of the diffractometer and the IP detectors has been given elsewhere (14, 15).

Since the neutron scattering length of Ti is negative, it is expected that the powder neutron diffraction data for $Pb_2(Ti_{1.5}W_{0.5})O_{6.5}$ will be relatively insensitive to changes in the positional and thermal parameters of the *B*-site cation. Coupled with this, the displacement of both the heavy Pb and light O atoms further limits the precision of the structural refinement from ND data. Consequently, the structural refinements used a combined neutron and X-ray diffraction data set in order to obtain precise and accurate structural descriptions of the material. The entire data set consisted of about 15,000 data points and 337 reflections. The Rietveld refinement (16) of the combined neutron and X-ray data was undertaken with the PC version of the computer program LHPM (17). For the neutron diffraction profile the background was defined by a fourth-order polynomial in 2θ and was refined simultaneously with the profile parameters. A Voigt function was chosen to generate the lineshape of diffraction peaks, in which the Gaussian component has widths given by the function (18) $(FWHM)^2 = U\tan^2\theta + V\tan\theta + W$, where U, V, and W are refinable parameters and the width of Lorentzian component was varied as $\eta\sec\theta$ to model particle size effect. The coherent scattering lengths used were Pb = 0.94017,

Sn = 0.62257, Ti = −0.3438, W = 0.477, and O = 0.5803 fm (19). For the X-ray diffraction profile the same background function was employed and a pseudo-Voigt function was chosen to generate the profile. Absorption was treated using the algorithm of Sabine and Dwiggins (20, 21).

XPS were recorded on Kratos XSAM 800 spectrometer by using Mg$K\alpha$ (1253.6 eV) radiation at 15 kV, 10 mA. The samples were presented as sintered disks. Spectra were recorded with a pass energy of 20 eV and all binding energies (BE) are referenced to the C 1*s* line at 284.6 eV. The spectra were fitted using pseudo-Voigt (50 : 50 Gaussian–Lorentzian) peak shape and a linear background. The sensitivity factors utilized were those supplied by the manufacturer (22).

RESULTS AND DISCUSSION

The two oxides were obtained as monophasic yellow microcrystalline powders. Electron micrographs demonstrated the materials to be highly crystalline and no unusual features were observed. The homogeneity and bulk composition of the samples was confirmed by EDA. As a consequence of the difference in the neutron scattering lengths of Ti and Sn the ND patterns of these two compounds show some dramatic differences (Fig. 1). For example, the 113 and 222 reflections (near 30°) have comparable intensity in $Pb_2(Ti_{1.5}W_{0.5})O_{6.5}$, whereas in $Pb_2(Sn_{1.5}W_{0.5})O_{6.5}$ the 113 reflection has almost zero intensity while the 222 reflection is among the strongest observed peaks. In $Pb_2(Ti_{1.5}W_{0.5})O_{6.5}$ since Ti and W have individual scattering lengths of opposite sign the effective scattering power of the B' site is small. In contrast, both Sn and W have large positive scattering lengths, and therefore the net contribution from the B' site is considerably larger in $Pb_2(Sn_{1.5}W_{0.5})O_{6.5}$.

Initial refinements of the structures, using the combined XRD and ND data sets, were carried out in space group $Fd\bar{3}m$ with atoms at the positions Pb, 16*d* (0.5, 0.5, 0.5); Sn/Ti/W randomly distributed on 16*c* (0, 0, 0); O on the 48*f* (*x*, 0.125, 0.125); and O′ on the 8*b* (0.375, 0.375, 0.375) sites and yielded *R* factors of $R_p = 1.63\%$, $R_{wp} = 3.35\%$ for $Pb_2(Ti_{1.5}W_{0.5})O_{6.5}$ and $R_p = 2.84\%$, $R_{wp} = 4.42\%$ for $Pb_2(Sn_{1.5}W_{0.5})O_{6.5}$. The refined oxygen positional parameters were 0.3150(1) for $Pb_2(Ti_{1.5}W_{0.5})O_{6.5}$ and 0.3196(3) for $Pb_2(Sn_{1.5}W_{0.5})O_{6.5}$. A recent study of the series of stannate pyrochlores $Ln_2Sn_2O_7$ (*Ln* = rare earth) revealed that the single variable oxygen positional parameter, *x*, systematically decreases as the cubic lattice parameter, *a*, increases (23). Comparison of available data for matched pairs of stannate and titanate pyrochlores shows a similar trend to be present. Similarly in the series $Y_2(Zr_yTi_{1-y})_2O_7$ as *a* increases, *x* decreases (24) and the observed value of *x*, 0.3065, in $Pb_2(TiSb)O_{6.5}$ $a = 10.4109(2)$ Å is smaller than that found in $Pb_2(Ti_{1.5}W_{0.5})O_{6.5}$ $a = 10.3392(1)$ Å. Thus the large difference in the value of *x* results from the relatively large difference in cell size.

The refined occupancies of the O′ site correspond to oxygen stoichiometries of 6.50(2) and 6.48(4) for *M* = Ti and Sn, respectively. Since vacancies at the *A* site can also occur in these types of materials, the occupancy of Pb cations was also refined, as were the occupancies of the *B*-site cations. In all cases these were found to be within 1 e.s.d. of the nominal stoichiometric values. Likewise no variations in the occupancies of the 48*f* (O) site was observed.

Close examination of the difference ND profiles for both compounds revealed several weak *hk*0 ($h + k \neq 4n$) and *h*00 ($h \neq 4n$) type lines, that are forbidden in space group $Fd\bar{3}m$, but are allowed in $F\bar{4}3m$. Consequently refinements were then undertaken in space group $F\bar{4}3m$ (No. 216). In the case of $Pb_2(Ti_{1.5}W_{0.5})O_{6.5}$ this led to an appreciable improvement in the fit while for $Pb_2(Sn_{1.5}W_{0.5})O_{6.5}$ the improvement was only marginal. The final positional, thermal, and occupancy parameters and the standard *R* factors are given in Table 1, and the best fits to the neutron diffraction data are shown in Fig. 1 while Fig. 2 shows the fit to the XRD data for $Pb_2(Sn_{1.5}W_{0.5})O_{6.5}$. In addition to altering the appearance of the neutron diffraction patterns the small scattering power on the *B* site in $Pb_2(Ti_{1.5}W_{0.5})O_{6.5}$ limits the precision in the positional and thermal parameters for the *B*-site atoms as shown by the higher e.s.d.'s. The structural refinements using the combined XRD and ND data sets significantly improved the precision of these parameters over refinements using only ND data. A further advantage of using the combined data sets is in the detection of substitution of Pb onto the *B* site. Attempts to refine models where small amounts of Pb were placed on the *B* site invariably resulted in a worsening of the fits.

The cubic lattice parameter of the Sn pyrochlore oxide is larger than that for the analogous Ti pyrochlore, in accord with the larger ionic radii of Sn^{4+} (0.83 Å) compared to Ti^{4+} (0.745 Å) (25). The average *M*/W–O bond distances are 1.95(2) and 2.02(1) Å for *M* = Ti and Sn, respectively, which are slightly smaller than the average Sn–O and Ti–O distances observed in the corresponding rutile-type dioxides (26). The *B*/*B*′ ions in $Pb_2(B_{2-x}B'_x)O_{6.5}$ are coordinated to three O(1) and three O(2) anions in a distorted octahedral geometry. These BO_6 octahedra then share corners to form a B_2O_6 3-dimensional network with hexagonal holes along the ⟨111⟩ direction. The increasing *B*/*B*′–O bond distances result in an increase in the size of this hole.

The Pb atoms are coordinated to seven oxygen anions forming a compressed scalenohedron, in which the eighth vertex is occupied by the $6s^2$ lone pair electrons (Table 2). There are two different Pb–O bond lengths; one short bond at 2.270(4) Å for *M* = Ti or 2.300(4) Å for *M* = Sn and six longer bonds at ca. 2.6–2.7 Å. The short Pb–O bond can be viewed as forming Pb_2O'-type chains where every second

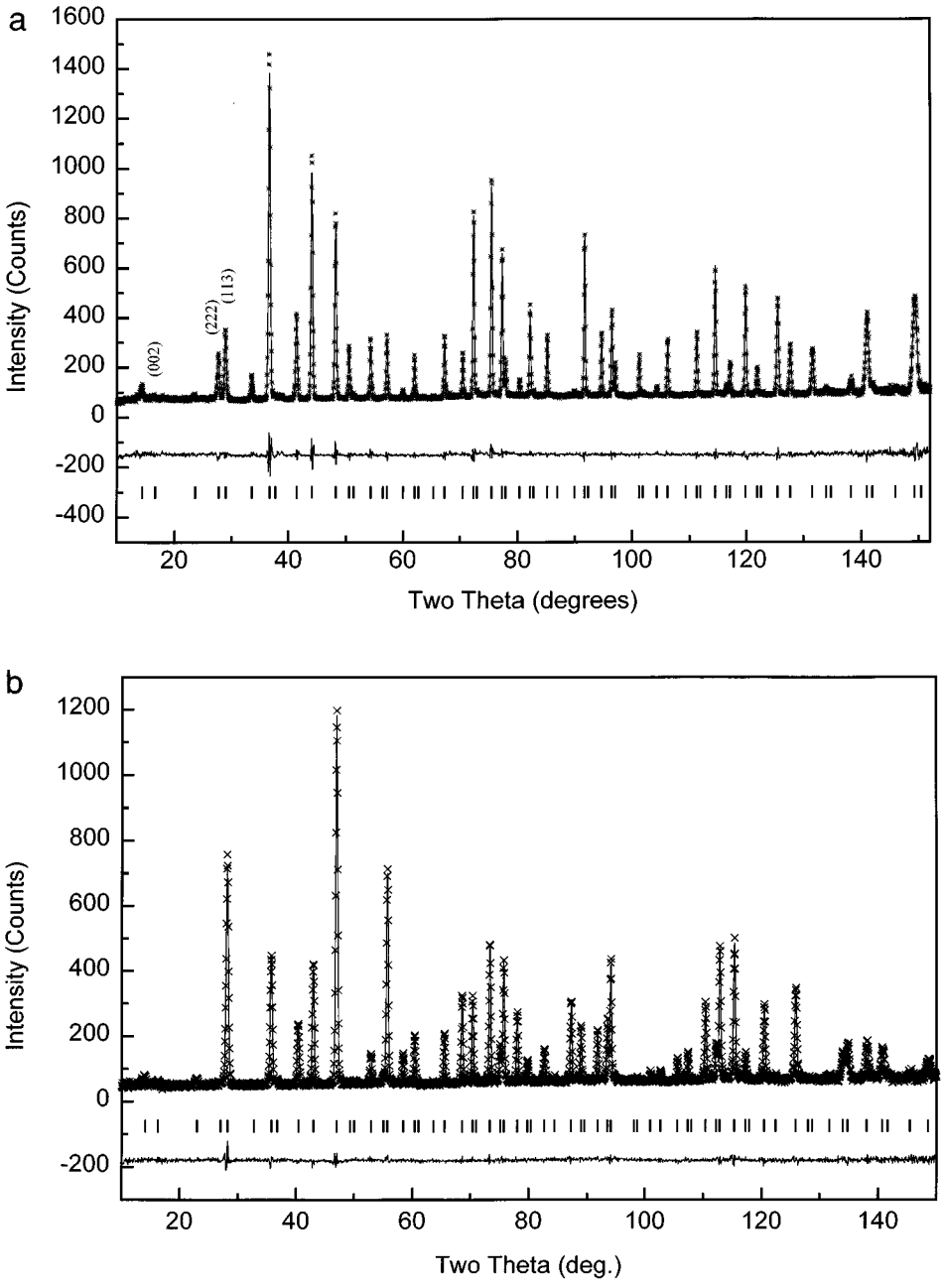

FIG. 1. Observed, calculated, and difference neutron powder diffraction profiles for (a) $Pb_2(Ti_{1.5}W_{0.5})O_{6.5}$ and (b) $Pb_2(Sn_{1.5}W_{0.5})O_{6.5}$. The observed data are indicated by crosses and the calculated profiles by the solid line. The short vertical lines below the profiles mark the position of all possible Bragg reflections. Note the presence of obvious (002) peak in both observed profiles which is forbidden in space group $Fd\bar{3}m$.

O′ site is vacant and sits at the center of a tetrahedron of lone pairs of electrons and these chains occupy the hexagonal holes of the B_2O_6 network. Previous structural studies of defect pyrochlores where oxygen vacancy ordering occurs have shown that the Pb atoms are displaced by up to 0.040 Å along the ⟨111⟩ direction toward the associated oxygen vacancy, thus lengthening the "short" Pb–O bond, and it has been suggested that this is necessary to fulfill the requirement of Pb–O bonding (4–6). A similar displacement is observed in the present work for $Pb_2(Ti_{1.5}W_{0.5})O_{6.5}$, where the Pb atoms are displaced 0.032(8) Å along the ⟨111⟩ direction. Conversely in the larger Sn oxide there is no significant displacement of Pb from the ideal position of (0.375, 0.375, 0.375), this being the equivalent of the 16*c* site

TABLE 1
Structural, Isotropic (Å²), and Anisotropic (10^3 Å²) Thermal and Occupation Parameters for $Pb_2Ti_{1.5}W_{0.5}O_{6.5}$ and $Pb_2Sn_{1.5}W_{0.5}O_{6.5}$[a]

$Pb_2(Ti_{1.5}W_{0.5})O_{6.5}$, $F\bar{4}3m$, $a = 10.3501(2)$ Å, $R_p = 1.52\%$, $R_{wp} = 2.88\%$

Atom	Site	x	occ.	B(Å²)[b]	u_{11}	u_{22}	u_{33}	u_{12}	u_{13}	u_{23}
Pb	16*e*	0.8767(4)	2.02(2)	1.41(2)	19.8(3)	u_{11}	u_{11}	− 5.1(4)	u_{12}	u_{12}
Ti	16*e*	0.3744(9)	1.46(4)	0.5(2)	19(1)	u_{11}	u_{11}	3(2)	u_{12}	u_{12}
W	16*e*	0.3744(9)	0.54(4)	0.5(2)	19(1)	u_{11}	u_{11}	3(2)	u_{12}	u_{12}
O(1)	24*f*	0.3101(4)	1	0.44(4)	4(2)	6(1)	u_{22}	0	0	− 5(2)
O(2)	24*g*	0.4407(4)	1	0.73(4)	10(2)	7(1)	u_{22}	0	0	2(2)
O(3)	4*d*	0.7500	0.94(6)	1.04(6)	16(1)	u_{11}	u_{11}	0	0	0

$Pb_2(Sn_{1.5}W_{0.5})O_{6.5}$, $F\bar{4}3m$, $a = 10.6051(2)$ Å, $R_p = 2.78\%$, $R_{wp} = 4.35\%$

Atom	Site	x	occ.	B(Å²)[b]	u_{11}	u_{22}	u_{33}	u_{12}	u_{13}	u_{23}
Pb	16*e*	0.8752(4)	1.98(2)	1.59(2)	20.6(3)	u_{11}	u_{11}	− 5.2(3)	u_{12}	u_{12}
Sn	16*e*	0.3754(4)	1.44(6)	0.40(2)	5.1(3)	u_{11}	u_{11}	− 0.5(4)	u_{12}	u_{12}
W	16*e*	0.3754(4)	0.56(6)	0.40(2)	5.1(3)	u_{11}	u_{11}	− 0.5(4)	u_{12}	u_{12}
O(1)	24*f*	0.3058(9)	1	1.06(5)	16(3)	12(1)	u_{22}	0	0	− 4(2)
O(2)	24*g*	0.4454(9)	1	1.25(5)	17(2)	12(1)	u_{22}	0	0	− 1(2)
O(3)	4*d*	0.7500	0.98(2)	0.55(6)	13(1)	u_{11}	u_{11}	0	0	0

[a] Number in parentheses are e.s.d.'s in the last significant digits.
[b] Values obtained for refinement isotropic thermal parameters. The inclusion of anisotropic thermal parameters did not significantly alter the structural and unit cell parameters.

at (0, 0, 0) in $Fd\bar{3}m$. The size of the hexagonal hole increases as the cell parameter increases and it appears that in $Pb_2(Sn_{1.5}W_{0.5})O_{6.5}$ the Pb–O bonding requirements can be fulfilled without any Pb displacement. Valence bond sum (VBS) calculations (27) show a decrease in the VBS of the Pb cations as the short Pb–O distance increases, the values being 2.1 and 1.9 for the Ti and Sn oxides, respectively. We suggest that bonding effects place an upper limit on the

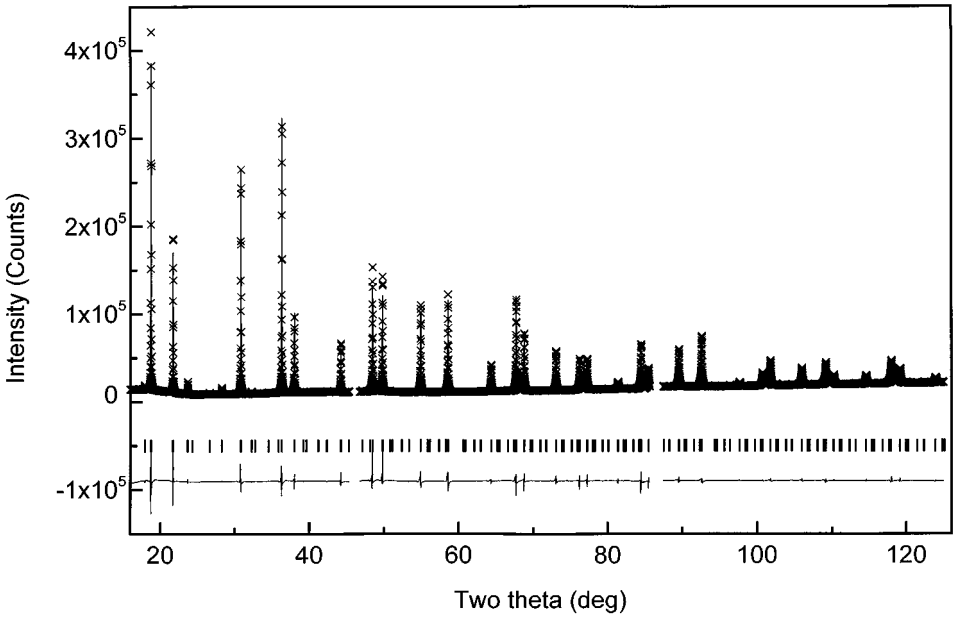

FIG. 2. Observed, calculated, and difference X-ray synchrotron diffraction profiles for $Pb_2(Sn_{1.5}W_{0.5})O_{6.5}$. The format is the same as in Fig. 1. The breaks in the profiles result from small gaps between the individual image plate detectors.

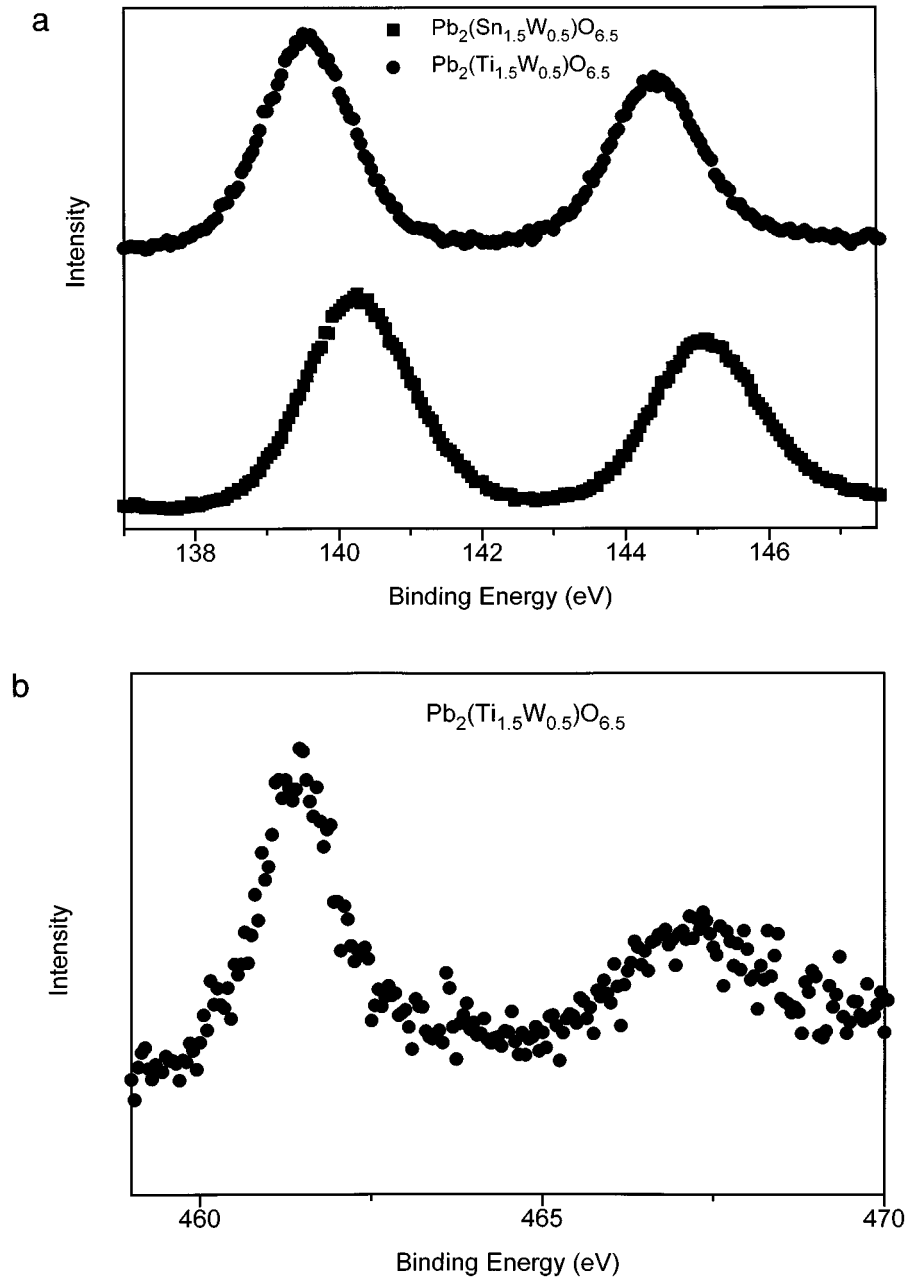

FIG. 3. Representative (a) Pb 4*f*, (b) Ti 2*p*, (c) Sn 3*d*, and (d) W 4*f* photoelectron spectra of $Pb_2(Ti_{1.5}W_{0.5})O_{6.5}$ (●) and $Pb_2(Sn_{1.5}W_{0.5})O_{6.5}$ (■).

Pb–O distance of about 2.30 Å in the present compounds and that such effects limit the displacement of the Pb cations.

For both compounds the thermal displacements of the heavier Pb cation are larger than those of the other lighter atoms. Similar features have been observed in a number of related pyrochlores (4–6) and for the Bi(2) atoms in $Bi_3M_3O_{11}$-type oxides (6, 11) that have a similar environment. The two short(S) and six long(L), or 1S and 6L, bonds in these moieties give the Pb/Bi atoms a relatively open coordination, and this in turn results in the large thermal displacements. The thermal motions of the Pb atoms are highly anisotropic and are described by the two principal vibrations, $u_{11} + 2u_{12}$ parallel to (111) direction and $u_{11} - u_{12}$ perpendicular to this. In $Pb_2(Ti_{1.5}W_{0.5})O_{6.5}$ the corresponding values are 8.4×10^{-3} and 24.9×10^{-3} Å^2, while for $Pb_2(Sn_{1.5}W_{0.5})O_{6.5}$ they are 9.8×10^{-3} and 25.8×10^{-3} Å^2, respectively, demonstrating that movement

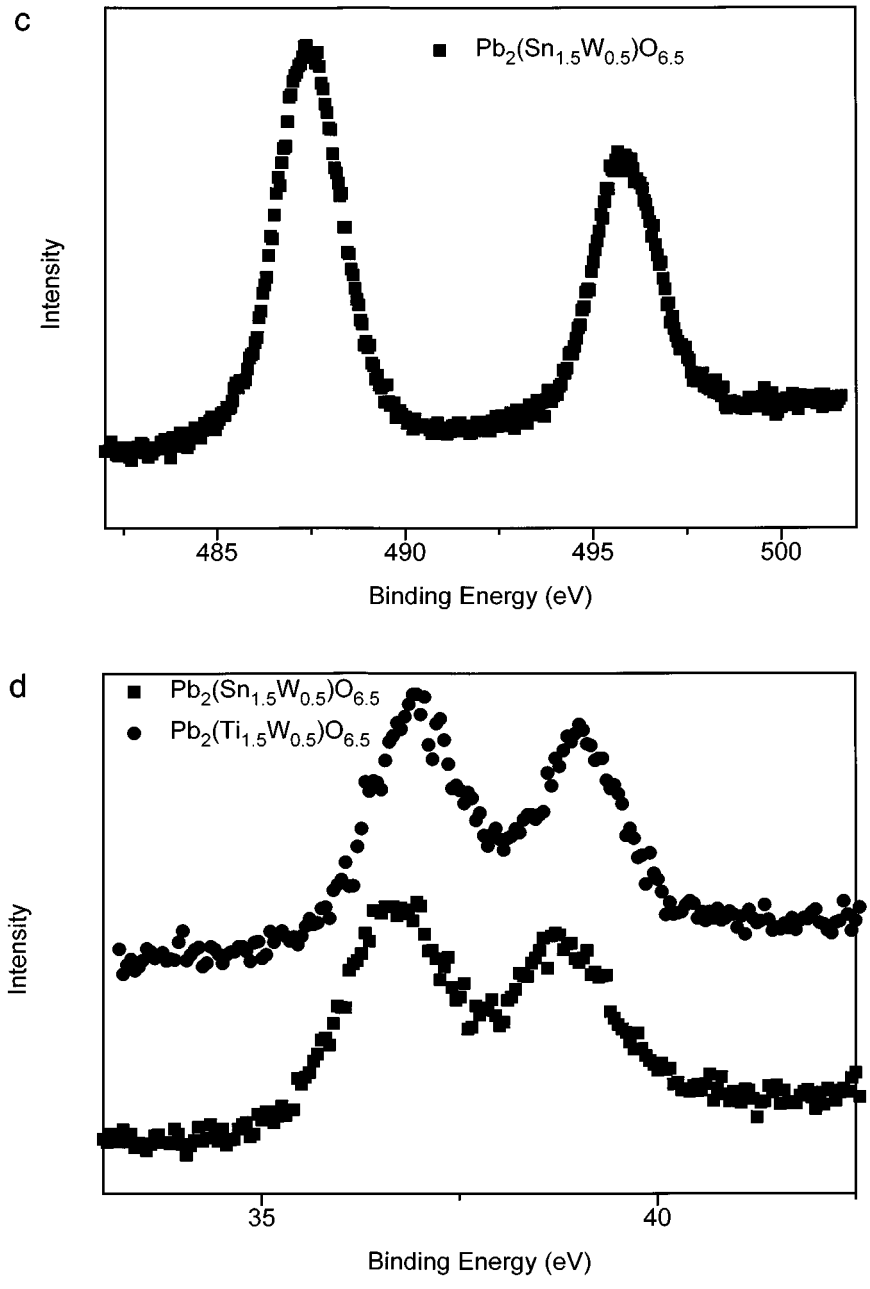

FIG. 3—*Continued*

along the $\bar{3}$ axis, i.e., toward the closest oxygen atom, is inhibited. This is a common feature of pyrochlore-type oxides (1) as a result of the local environment of the Pb cations. Comparison of these results with those obtained in other pyrochlore oxides demonstrates that anion vacancy ordering has little effect on the magnitude of the thermal displacements. The thermal parameters of the M/W atoms do not show any appreciable anisotropy.

X-ray photoelectron spectra of both compounds revealed no surface impurities. In all cases the various diagnostic spectral manifolds appear as symmetric doublets (Fig. 3). The Pb $4f_{7/2}$ line in both compounds has a binding energy (BE) of about 139 eV (Table 3). Although the Pb 4*f* BEs are generally regarded as being insensitive to oxidation state, as illustrated by the Pb $4f_{7/2}$ BE of PbO_2 and PbO being 138.4 and 138.1 eV, respectively, previous studies of metallic Pb(II)-containing pyrochlores have shown that the Pb $4f_{7/2}$ BE attributed to Pb(II) in the A site of the pyrochlore lattice is generally lower than this, $\sim$ 137 eV. This can be readily distinguished from nonpyrochlore surface oxides (6, 10, 11).

TABLE 2
Selected Bond Distances (Å) in Some $Pb_2(B_{2-x}B'_x)O_{6.5}$ Compounds

Compound	a (Å)	Octahedral environment		Scalenohedral environment			
		M–O(1) 3×	M–O(2) 3×	Pb–O(1) 3×	Pb–O(2) 3×	Pb–O(3) 1×	Pb–V[d] 1×
$Pb_2Ru_2O_{6.5}$[a]	10.2519(2)	1.954(4)	1.969(4)	2.564(2)	2.563(2)	2.260(2)	2.180(2)
$Pb_2Ir_2O_{6.5}$[b]	10.26450(4)	1.968(4)	1.985(4)	2.544(2)	2.546(2)	2.267(2)	2.178(2)
$Pb_2(Ti_{1.5}W_{0.5})O_{6.5}$	10.3392(1)	1.971(9)	1.946(9)	2.642(5)	2.645(5)	2.270(4)	2.207(4)
$Pb_2(TiSb)O_{6.5}$[c]	10.4109(2)	1.982(20)	1.966(20)	2.634(4)	2.643(4)	2.294(3)	2.215(3)
$Pb_2(Sn_{1.5}W_{0.5})O_{6.5}$	10.60756(8)	2.010(5)	2.023(5)	2.681(8)	2.673(6)	2.300(4)	2.293(4)

[a] From reference 6.
[b] From reference 8.
[c] From reference 7.
[d] Vacancy.

In the present oxides the Pb $4f_{7/2}$ BE is about 2 eV higher than that observed in $Pb_2Ru_2O_{6.5}$ and $Pb_2Ir_2O_{6.5}$. Although the BE of an element is often used as a guide to the oxidation state, it is in fact a direct measure of electron density on a particular atom, and as such, various electronic interactions can result in species with the same formal oxidation state having dramatically different BE (28). The difference in the Pb $4f$ BE in the metallic, Ru, and Ir pyrochlores, and the present nonmetallic Sn/Ti pyrochlore oxides is related to the difference in bonding in these oxides. The higher Pb $4f$ BE in the two nonmetallic oxides is explained by a lower degree of covalency in these compounds compared to the Ir and Ru analogs. This difference in bonding is clearly illustrated by VBS calculations that show that Pb VBS values in $Pb_2Ru_2O_{6.5}$ and $Pb_2Ir_2O_{6.5}$ are comparable, $\sim$2.4, and dramatically higher than values found in $Pb_2(Ti_{1.5}W_{0.5})O_{6.5}$ and $Pb_2(Sn_{1.5}W_{0.5})O_{6.5}$ $\sim$2.0. Thus the Pb $4f_{7/2}$ lines at ca. 139 eV are assigned to Pb^{2+} ions in pyrochlore A site in the absence of metallic bonding. In the present case the halfwidths of the Pb $4f$ lines show no unusual broadening demonstrating that the Pb electrons are localized and there is no indication for any other Pb species being present. This is in agreement with the bulk diffraction studies that showed there to be no Pb vacancies or site disorder and that the only crystalline Pb-containing species present was oxygen defect pyrochlore. The Sn $3d$ spectral manifold is also relatively insensitive to oxidation state. The symmetric peak shapes of both $3d_{5/2}$ and $3d_{3/2}$ lines suggest that a single Sn species is present. A similar conclusion can be made for Ti $2p$ and W $4f$ manifolds where the observed BE are consistent with the expected Ti^{4+} and W^{6+} oxidation states.

Quantification of the surface composition demonstrates that, unlike the case of metallic $Pb_2Ru_2O_{6.5}$ and $Pb_2Ir_2O_{6.5}$ where appreciable surface enrichments by Pb occurs, there is no surface enrichment in the present nonmetallic pyrochlore oxides (Table 3). The present oxides show both anion-vacancy ordering and large thermal parameters for the A site cations. The latter suggests some disorder of the A site cations indicative of mobility. Naively it might therefore be expected that the materials would show some surface enrichment by the weakly bonded A cations as a result of diffusion through the large channels in the pyrochlore lattice. That this is not observed provides further evidence for some form of coupling between the electrical conductivity and ionic mobility in pyrochlore-type metal oxides.

TABLE 3
XPS Data for $Pb_2(M_{1.5}W_{0.5})O_{6.5}$ (M = Ti, Sn)

M	Pb $4f_{7/2}$ (eV)	Δ[a]	Γ[b]	Ti $2p_{3/2}$ (eV)	Δ	Γ	Sn $3d_{3/2}$ (eV)	Δ	Γ	W $4f_{7/2}$ (eV)	Δ	Γ	Pb : M : W
Ti	140.1	4.9	1.4	459.7	5.8	1.5				37.0	2.1	1.4	2 : 1.5 : 0.5
	145.0		1.5	465.5		2.8				39.1		1.4	
Sn	139.6	4.9	1.5				487.4	8.5	1.6	36.6	2.2	1.2	2 : 1.6 : 0.4
	144.5		1.6				495.9		1.6	38.8		1.4	

[a] Separation between spin orbit doublets.
[b] Full width at half-maximum height.

ACKNOWLEDGMENTS

This work has been supported by Australian Institute of Nuclear Science and Engineering, Australian Research Council, and Australian National Beamline Facility.

REFERENCES

1. M. A. Subramanian, G. Aravamudan, and G. V. Subba Rao, *Progr. Solid State Chem.* **15,** 55 (1983).
2. Y. Shimakawa, Y. Kubo, and T. Manako, *Nature* **379,** 53 (1996).
3. R. A. Beyerlein, H. S. Horowitz, and J. M. Longo, *J. Solid State Chem.* **72,** 2 (1988).
4. R. A. Beyerlein, H. S. Horowitz, J. M. Longo, M. E. Leonowitz, J. A. Jorgensen, and F. J. Rotella, *J. Solid State Chem.* **51,** 253 (1984).
5. J. A. Alonso, C. Cascales, I. Rasines, and J. Pannetier, *Acta Crystallogr. C* **45,** 3 (1989).
6. B. J. Kennedy, *J. Solid State Chem.* **123,** 14 (1996).
7. G. R. Facer, M. M. Elcombe, and B. J. Kennedy, *Aust. J. Chem.* **46,** 1897 (1993).
8. G. Gokagac and B. J. Kennedy, *J. Electroanal. Chem.* **353,** 71 (1993).
9. G. Gokagac and B. J. Kennedy, *J. Electroanal. Chem.* **368,** 235 (1994).
10. Ismunandar, B. J. Kennedy, and B. A. Hunter, *J. Solid State Chem.*, in press.
11. I. N. Belyaev, L. N. Aver'yanova, and I. I. Belyaeva, *Kristalografiya* (*Eng. trans.*) 220 (1964).
12. Wakiya, *Mater. Res. Bull.* **28,** 137 (1993).
13. C. J. Howard, C. J. Ball, R. L. Davis, and M. M. Elcombe, *Aust. J. Phys.* **36,** 507 (1983).
14. Z. Barnea, D. C. Creagh, T. J. Davis, R. F. Garret, S. Janky, A. W. Stevenson, and S. W. Wilkins, *Rev. Sci. Instrum.* **63,** 1069 (1992).
15. R. F. Garret, D. J. Cookson, G. J. Foran, T. M. Sabine, B. J. Kennedy, and S. W. Wilkins, *Rev. Sci. Instrum.* **66,** 1351 (1995).
16. H. M. Rietveld, *J. App. Crystallogr.* **2,** 65 (1969).
17. R. J. Hill and C. J. Howard, Australian Atomic Energy Commision Report No. M112, AAEC(now ANSTO), Lucas Heights Researchs Laboratories, New South Wales, Australia, 1986.
18. G. Caglioti, A. Paeloetti, and F. P. Ricci, *Nucl. Instrum.* **3,** 223 (1958).
19. V. F. Sears, Atomic Energy of Canada Limited Report AECL-8490, 1984.
20. T. M. Sabine and W. R. Sabine, submitted for publication.
21. C. W. Dwiggins, *J. Appl. Crystallogr.* **13,** 572 (1980).
22. "Vision Reference Manual," Kratos, UK.
23. B. J. Kennedy, B. A. Hunter, and C. J. Howard, accepted for publication.
24. C. Heremans, B. J. Wuensch, J. K. Stalick, and E. Prince, *J. Solid State Chem.* **117,** 108 (1995).
25. R. D. Shannon, *Acta Crystallogr.* **32,** 751 (1976).
26. A. Bolzan, C. Fong, B. J. Kennedy, and C. J. Howard, *Acta Crystallogr.*, in press.
27. N. E. Breese and M. O'Keeffe, *Acta Crystallogr. B* **47,** 192 (1991).
28. D. Briggs and M. P. Seah, "X-Ray Photoelectron Spectroscopy, Vol. 1, Auger and X-ray Photoelectron Spectroscopy," Wiley, New York, 1983.